

Intrinsic (non)-Gilbert damping in magnetic insulators calculated from a minimal model and *ab initio* spin Hamiltonians.

Andrei Shumilin,* Diego López-Alcalá, Nassima Benchtaber, Alberto M. Ruiz, and José J. Baldoví†
Instituto de Ciencia Molecular, Universitat de València, 46980 Paterna, Spain

We present an analytically solvable minimal model for the relaxation of low-frequency magnons in magnetic insulators arising from magnon–phonon and magnon–magnon interactions. The model establishes a direct connection between microscopic relaxation processes and Gilbert damping, and reveals how magnon decay evolves from bulk systems to the monolayer limit. We find that magnon–phonon coupling produces Gilbert damping of comparable magnitude in three- and two-dimensional magnets, with qualitative differences between flexural phonons in free-standing monolayers and three-dimensional phonons in substrate-supported layers. By contrast, non-Gilbert damping due to four-magnon scattering is strongly enhanced in two dimensions, where it becomes independent of spin–orbit coupling. To benchmark the model against real materials, we introduce a numerical approach for computing magnon damping from *ab initio*–derived spin Hamiltonians. We demonstrate that the central conclusions of the model remain valid for magnons in bulk YIG and in a monolayer of the van der Waals magnetic insulator CrSBr.

I. INTRODUCTION

Magnonics is a rapidly advancing branch of magneto-electronics and spintronics that focuses on the generation, control, and detection of magnons—the quanta of spin waves [1, 2]. It offers a versatile platform for investigating fundamental spin phenomena and enables a broad range of device concepts, including low-power information processing [3] and artificial neural networks [4]. Early developments in magnonics relied primarily on relatively thick magnetic films combined with macroscopic magnon antennas [5]. However, the ongoing trend toward miniaturization has opened new possibilities, including quasi-two-dimensional (2D) van der Waals (vdW) magnets, which retain magnetic order down to the monolayer limit [6].

Despite this progress, a major challenge common to all magnonic technologies is the relaxation (or damping) of spin waves. This relaxation is most commonly incorporated into the Landau–Lifshitz–Gilbert (LLG) equation—the standard framework for spin-wave simulations—via the Gilbert damping parameter α [7, 8]. Although several strategies for magnon amplification have been proposed [9–11], low damping remains a key requirement for practical magnonic materials. This requirement has made yttrium iron garnet (YIG), with its exceptionally low damping $\alpha < 10^{-4}$, the prototypical magnonic material [12–15]. Nevertheless, the search for novel low-damping materials continues, with several promising candidates proposed [16], including vdW layered magnets [17, 18]. Since Gilbert damping is often associated with spin–orbit coupling (SOC) [19–21], materials with weak SOC represent an appealing direction for this search.

Experimentally, the damping parameter α is most commonly extracted from ferromagnetic resonance

(FMR) measurements via the magnetic-field dependence of the linewidth. The FMR linewidth typically consists of two main contributions: an inhomogeneous component related to material nonuniformity and independent of frequency, and a homogeneous component associated with magnon decay [22]. If the decay is governed by Gilbert damping, the homogeneous linewidth is proportional to the FMR frequency, enabling its separation from the inhomogeneous contribution. However, several experimental studies have reported deviations from this so-called Gilbert behavior [23–25], including linewidths that decrease with increasing FMR frequency [14]. One well-known source of such non-Gilbert behavior is two-magnon scattering induced by impurities or surface roughness [26–28]. Beyond FMR, spin-wave decay can also be probed directly using time-resolved techniques, which allow the relaxation rate to be determined independently of its frequency dependence [29–31].

In many experimental situations, the measured damping is dominated by extrinsic effects arising from disorder or impurities in the material [32, 33]. Nevertheless, intrinsic damping is of fundamental importance, as it represents the theoretical lower bound attainable in a perfect crystal. Three intrinsic damping mechanisms are commonly identified: magnon–electron, magnon–phonon, and magnon–magnon scattering. Among these, magnon–electron scattering—which describes energy transfer from magnons to itinerant electrons—has been studied most extensively. It can be evaluated using several *ab initio* approaches [20, 34] and typically yields damping values $\alpha \sim 10^{-3}$ [35, 36]. However, the most promising low-damping magnonic materials, including YIG, are electrical insulators and therefore free from magnon–electron scattering.

Magnon–phonon interactions have been theoretically investigated in several works [37–41], with some of these studies enabling the extraction of phonon-induced contributions to the Gilbert damping in YIG [40, 41]. Magnon–magnon scattering has likewise been exam-

* andrei.shumilin@uv.es

† J.Jaime.Baldovi@uv.es

ined [42, 43], often with particular emphasis on antiferromagnetic systems [44, 45]. However, these studies typically focus on specific materials and frequently address magnons at large wave vectors, whereas Gilbert damping is defined in the low-wavevector limit. Consequently, a unified understanding of which intrinsic damping mechanisms dominate in a given insulating material—and how their relative importance evolves from bulk systems to the monolayer limit—remains lacking.

In this Letter, we present a systematic study of intrinsic damping mechanisms in magnetic insulators, with particular emphasis on the differences between two- and three-dimensional (2D and 3D) materials and comparison with LLG. We apply the Boltzmann formalism, which is widely used in the theory of magnon relaxation [40, 41, 43] and is expected to be valid when the magnon decay rate is small compared to its frequency [46], which in our case corresponds to the condition $\alpha \ll 1$. We first introduce a minimal toy model that allows for an analytical treatment of both magnon–magnon and magnon–phonon damping in 2D and 3D systems. We then perform numerical calculations for bulk YIG and for a monolayer of the vdW magnetic insulator CrSBr, demonstrating that the key results obtained from the model remain applicable to realistic materials.

II. GENERAL THEORY AND THE MINIMAL TOY MODEL

We consider a magnetic material described with a generalized spin Hamiltonian

$$H = - \sum_{i,j} \mathbf{S}_i \hat{J}_{ij} \mathbf{S}_j - \sum_i \mu_B g_i \mathbf{S}_i \cdot \mathbf{B} - \sum_{i,j;k} \mathbf{S}_i \frac{\partial \hat{J}_{ij}}{\partial \mathbf{r}_k} \mathbf{S}_j \mathbf{u}_k. \quad (1)$$

Here \mathbf{S}_i denotes the vector of spin operators associated with a magnetic atom i , and g_i is the corresponding Lande g -factor. The tensor \hat{J}_{ij} describes the exchange interaction between magnetic atoms i and j . While in the non-relativistic limit, \hat{J}_{ij} reduces to a scalar, in the general case it becomes a full 3×3 matrix in Cartesian coordinates [47]. In this general form, \hat{J}_{ij} can account both for the exchange interaction, including its anisotropic part, and magnetic dipole–dipole interactions. μ_B is the Bohr magneton and \mathbf{B} denotes the external magnetic field. To account for the interaction with phonons, we consider the modulation of the exchange tensor \hat{J}_{ij} due to the atomic displacement \mathbf{u}_k , where the index k runs over all the atoms of the system. $\partial \hat{J}_{ij} / \partial \mathbf{r}_k$ is the derivative of the exchange tensor \hat{J}_{ij} over the position of atom k . Close to the ground state, Eq. (1) can be mapped onto a quasiparticle Hamiltonian using the Holstein–Primakoff transformation [48] and the second-quantization of the displacements \mathbf{u}_k . The resulting quasi-particles are treated with Boltzmann equation.

We consider an initial excitation of a classical long-wavelength spin-wave corresponding to a macroscopically

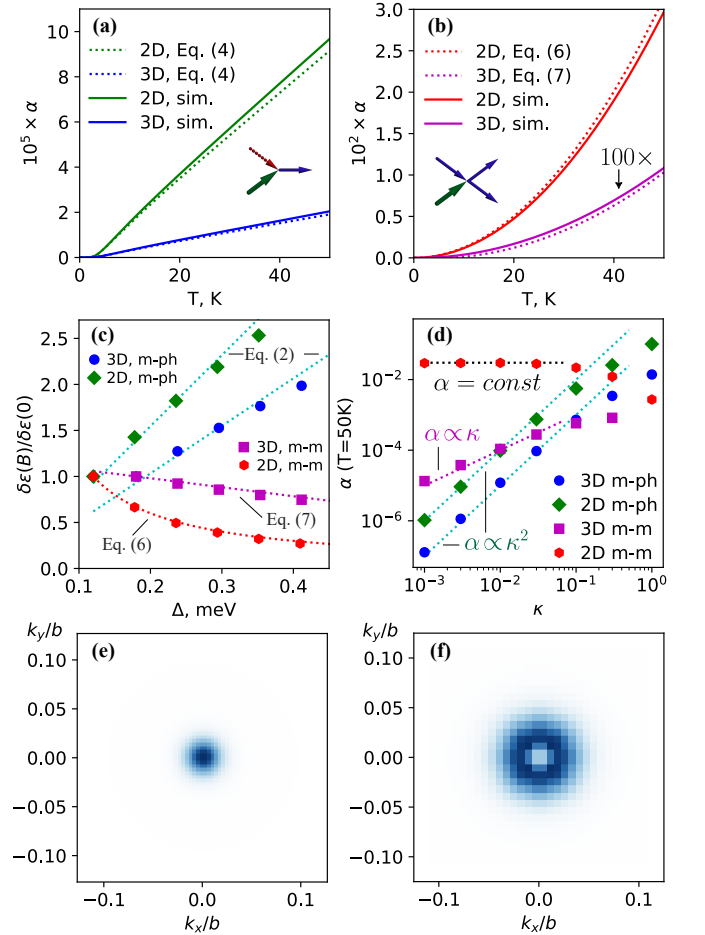


FIG. 1. Magnon damping in the minimal toy model. (a) Temperature dependence of the damping due to the magnon-phonon interaction. (b) Temperature dependence of the damping due to the magnon-magnon interaction. (c) Magnon linewidth dependence on the energy compared with the Gilbert law (red solid lines) and with the non-Gilbert behavior derived from Eqs. (6) and (6), black dashed and dashed-dotted lines, respectively. (d) Dependence of the damping parameter α in zero magnetic field on the anisotropy parameter κ . (e,f) distribution of the magnons responsible for the magnon-magnon induced damping in 2D and 3D models, respectively.

large occupation number N_0 of $\mathbf{k} \rightarrow 0$ acoustic magnons. The occupation numbers of all other quasiparticles are thermal and follow the Bose–Einstein distribution. The relaxation of the initial spin-wave is described by the relaxation rate γ_0 which is directly related to the homogeneous linewidth in FMR experiments $\delta\varepsilon = \hbar\gamma_0$.

An equivalent treatment of the same physical problem within LLG formalism yields the relation

$$\gamma_0 = \alpha\Delta/\hbar \quad (2)$$

where Δ denotes the energy of the $\mathbf{k} = 0$ acoustic magnons (the magnon gap), and α is the dimensionless Gilbert damping parameter.

To provide a unified description of both Gilbert and non-Gilbert magnon relaxation, we define the dimensionless damping parameter as $\alpha = \hbar\gamma_0/\Delta$ which can be evaluated at zero or finite external magnetic field. Within this framework, we distinguish between Gilbert damping, for which α is field-independent at least in small magnetic fields, and non-Gilbert damping corresponding to the relation (2) being broken at any values of B .

We begin our analysis from a minimal toy model, which consists of a square lattice in 2D or a cubic lattice in 3D, with lattice constant a , magnetic atoms of spin S , and atomic mass m . We assume the ferromagnetic exchange interactions between nearest-neighbors:

$$\mathbf{S}_i \hat{J}_{ij} \mathbf{S}_j = J \left(\mathbf{S}_i \cdot \mathbf{S}_j + \kappa S_i^{(z)} S_j^{(z)} \right). \quad (3)$$

Here J denotes the Heisenberg exchange coupling and κJ represents a small uniaxial anisotropy along the z axis.

The lattice dynamics is modeled by three acoustic phonon branches with identical sound velocity c . The exchange interaction is assumed to depend solely on the distance between neighboring atoms, and its modulation due to atomic displacements is characterized by a derivative $dJ/dr = J'$. The anisotropy parameter κ is independent of atomic displacements.

Within this model, both damping mechanisms allow analytical treatment when temperature T is large compared to Δ . The magnon-phonon interaction contributes to the damping via the processes when the $\mathbf{k} = 0$ acoustic magnon absorbs a phonon with a wavevector \mathbf{q} . The resulting expression for the Gilbert damping is [49]

$$\alpha_{m-ph} = 2D \frac{k_1^{D-2} a^D (\kappa S J')^2}{(2\pi)^{D-1} \Delta_0 m c^2} \times [M(k_1) - N(k_1)] \mathcal{J}_D(k_1 a). \quad (4)$$

Here D is the dimensionality of the system. $k_1 = \hbar c / JS a^2$ is the phonon wave vector that satisfies the energy and momentum conservation laws. The quantities $M(k_1)$ and $N(k_1)$ denote the Bose-Einstein occupation numbers of phonons and magnons, respectively. $\Delta_0 = 2D\kappa JS$ is the magnon gap at zero external magnetic field. The functions $\mathcal{J}_2(x)$ and $\mathcal{J}_3(x)$ are given by the expressions:

$$\begin{aligned} \mathcal{J}_2(x) &= \int_0^{2\pi} \sin^2(x \cos(\phi)) d\phi \approx \pi x^2 \\ \mathcal{J}_3(x) &= (2\pi/x)(x - \cos(x) \sin(x)) \approx 4\pi x^2/3 \end{aligned} \quad (5)$$

The r.h.s. of Eqs. (5) corresponds to the condition $x \ll 1$.

Fig. 1(a) shows the temperature dependence of the magnon damping calculated with Eq. (4) compared with the numerical simulations of 2D and 3D model. The model parameters are: $J = 2 \text{ meV}$, $\kappa = 0.01$, $a = 3 \text{ \AA}$, $c = 910 \text{ m/s}$, $m = 1 \text{ a.e.m.}$; $J' = -J/a$. The damping is suppressed at $T < \hbar c k_1$ and grows linearly with temperature at larger values of T . It is somewhat larger in 2D case reaching $\sim 10^{-4}$ at a temperature of 50 K, however, the results for both the 2D and 3D cases are comparable in order of magnitude.

The magnon-magnon interaction contributes to the damping via the 4-magnon process when the $\mathbf{k} = 0$ magnon interacts with another magnon with a wavevector \mathbf{k}_1 , resulting in two new magnons with wavevectors \mathbf{k}_2 and \mathbf{k}_4 , respectively. The corresponding contributions to α are [49]:

$$\alpha_{m-m}^{(2D)} = \frac{1.35 T^2 \Delta_0^2}{(2\pi JS^2)^2 \Delta^2}, \quad (6)$$

$$\alpha_{m-m}^{(3D)} = \frac{\Delta_0^2 T^2}{(2\pi JS^2)^3 \Delta} \left(0.82 - 2.94 \frac{\Delta}{T} \right). \quad (7)$$

These equations include the quadratic temperature dependence of α as shown in Fig. 1(b). The damping is very strong in 2D case reaching ~ 0.03 at $T = 50 \text{ K}$. Nevertheless, it is ~ 300 times weaker in the 3D case.

Both in 2D and 3D model the magnon-phonon contribution to the damping follow the Gilbert law (2) as shown in Fig. 1(c), where we present the FMR linewidth calculated in external magnetic fields up to 1.25 T and normalized to its value at zero magnetic field. However, the magnon-magnon contribution for both the dimensionalities is non-Gilbert due to the explicit dependence of $\alpha_{m-m}^{(2D)}$ and $\alpha_{m-m}^{(3D)}$, described by Eqs. (6) and (7), respectively, on Δ . In both the cases, the linewidth $\delta\varepsilon$ decreases with Δ as shown in Fig. 1(c). In 2D it follows the power law $\delta\varepsilon \propto \Delta^{-1}$ while in 3D this decrease is somewhat weaker.

The strong damping due to the magnon-magnon mechanism in the 2D model is related to $\alpha_{m-m}^{(2D)}$ described by Eq. (6) being independent of the anisotropy parameter κ at zero external field. To illustrate this we show in Fig. 1(d) the damping calculated from both the mechanisms in 2D and 3D models with varying κ and other parameters corresponding to Figs. 1(a-c). For relatively large values of κ all the mechanisms lead to comparable damping parameters. Nevertheless, at small κ the magnon-phonon-induced α decreases as $\alpha \propto \kappa^2$, magnon-magnon mechanism in 3D yields a slower decrease $\alpha \propto \kappa$ and in 2D it leads to $\alpha \approx \text{const}$.

As shown in Appendix A, the non-Gilbert damping derived from the Boltzmann equation is governed by low-energy quasiparticles participating in scattering processes. Figures 1(e) and (f) display the contributions of magnons with different wavevectors \mathbf{k}_1 to the magnon-magnon damping mechanism in 2D and 3D toy models, respectively. In both cases, the damping is dominated by low- $|\mathbf{k}_1|$ magnons with energies close to the magnon gap, whose strong field dependence leads to non-Gilbert behavior. However, owing to the different magnon statistics in two and three dimensions, the contribution vanishes exactly at $\mathbf{k}_1 = 0$ in the 3D case [Fig. 1(f)], while no such suppression occurs in 2D [Fig. 1(e)], rendering the non-Gilbert behavior less pronounced in three dimensions.

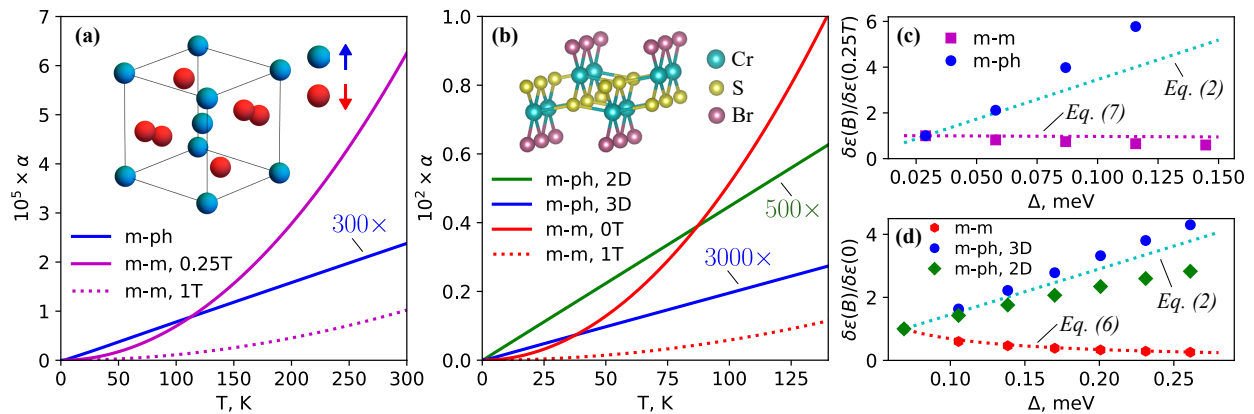


FIG. 2. Magnon damping calculated from *ab initio* spin Hamiltonians. (a) Temperature-dependent damping in bulk YIG arising from magnon–magnon (m–m) interactions at $B = 0.25$ T and $B = 1$ T, and from magnon–phonon (m–ph) interactions. Inset shows the positions of spin-up and spin-down Fe atoms in an $1/8$ of YIG cubic cell. (b) Temperature-dependent damping in a CrSBr monolayer due to magnon–magnon (m–m) interactions at $B = 0$ and $B = 1$ T, and due to magnon–phonon (m–ph) interactions with both 2D and 3D phonons. The inset illustrates the monolayer crystal structure. (c) FMR linewidth $\delta\varepsilon$ in YIG, normalized to its value at $B = 0.25$ T. The m–ph and m–m contributions are compared with the Gilbert damping and with Eq. (7), respectively. (d) FMR linewidth $\delta\varepsilon$ in a CrSBr monolayer, normalized to its value at $B = 0$. The m–ph and m–m contributions are compared with the Gilbert damping and with Eq. (6), respectively. Results for both 2D and 3D phonons are shown, as indicated in the legend.

III. MODELING OF REAL MATERIALS

To show that the results derived from the minimal model are relevant for real materials we provide the numeric calculations of the damping for the spin Hamiltonians extracted from the *ab initio* simulation of two materials relevant for magnonics: bulk YIG and a monolayer of CrSBr [17]. The calculations are performed with our *MagnoFallas* code, which is described in details in Appendix B and in the supporting information (SI) [49].

Yttrium iron garnet (YIG) is a ferrimagnetic insulating oxide crystallizing in the cubic centrosymmetric space group $Ia\bar{3}d$. Its magnetic order arises from two antiferromagnetically coupled Fe^{3+} sublattices (octahedral and tetrahedral sites) with unequal occupation (24 and 16 Fe ions per cubic unit cell), leading to a finite net magnetization despite the antiparallel spin alignment (see inset of Fig. 2(a)). The temperature dependence of magnon–magnon and magnon–phonon damping in bulk YIG, including both magnon-conserving and magnon-nonconserving contributions (see Appendix A), is shown in Fig. 2(a). The results are consistent with predictions of the toy model: magnon–magnon damping is stronger and exhibits a quadratic temperature dependence, whereas magnon–phonon damping varies linearly with temperature. To assess the Gilbert or non-Gilbert character of the damping, we evaluate the dependence of the calculated FMR linewidth $\delta\varepsilon$ on the energy Δ of the $\mathbf{k} = 0$ acoustic magnon mode. The results, shown in Fig. 2(c), are normalized to the linewidth at an external field of 0.25 T. Note that at zero field the long-range dipole–dipole interaction renders the macroscopic ferromagnetic state of YIG unstable. The linewidth

arising from magnon–phonon scattering follows Eq. (2) at low magnetic fields, allowing the damping to be classified as Gilbert, although deviations from Eq. (2) emerge at higher fields. In contrast, damping due to magnon–magnon scattering is distinctly non-Gilbert and is instead well described by Eq. (7) derived from the toy model.

Monolayer CrSBr is a ferromagnetic semiconductor that adopts an orthorhombic crystal structure belonging to the Pmmm space group. Within each layer, the Cr atoms reside in a distorted octahedral coordination environment. Along the a axis, neighboring Cr atoms are linked through both sulfur and bromine atoms, whereas along the b and c directions the Cr atoms are interconnected solely via sulfur atoms [17, 50, 51], as shown in the inset in Fig. 2(b).

Before discussing the simulation results for this monolayer, we note that thin films of vdW materials can be prepared either as free-standing layers or grown on a substrate. This distinction can significantly modify the phonon dispersion and, consequently, the phonon-induced damping. To account for this effect, we perform two sets of simulations: in the first, the phonons are treated as two-dimensional (2D) and derived from the monolayer itself; in the second, the (3D) phonon spectrum is taken from bulk CrSBr, while magnetic atoms and exchange interactions are still restricted to a single monolayer. Figure 2(b) shows that the temperature dependence of the magnon–phonon damping is linear in both cases; however, the damping is approximately an order of magnitude stronger for two-dimensional phonons. This enhancement arises because two-dimensional phonons allow energy and momentum

conservation to be satisfied at much smaller magnon energies, as discussed in Appendix C. The damping due to magnon–magnon interactions exhibits a quadratic temperature dependence and is substantially stronger than the magnon–phonon contribution.

Figure 2(d) shows the $\delta\varepsilon(\Delta)$ dependence in a CrSBr monolayer. In agreement with the toy model, the damping originating from magnon–phonon scattering is Gilbert for both phonon dispersions considered, whereas the damping due to magnon–magnon scattering is non-Gilbert and follows Eq. (6).

IV. DISCUSSION AND CONCLUSIONS

Our results demonstrate that strong non-Gilbert damping originating from magnon–magnon scattering emerges generically in two-dimensional magnetic systems and is not suppressed by weak spin–orbit interaction. This behavior is observed both in the toy model and in the spin Hamiltonian derived from *ab initio* calculations for a CrSBr monolayer.

At the level of the Boltzmann equation, this effect can be traced to small scattering matrix elements W_{if} being compensated by the large occupation numbers of low-energy thermal magnons. However, as shown in Appendix D, the same mechanism persists in an antiferromagnetic toy model with a magnon dispersion and statistics, qualitatively different from the ones in ferromagnetic materials. We therefore suppose that the origin of this behavior might be more fundamental. In three-dimensional Heisenberg magnets, the $\mathbf{k} = 0$ acoustic magnons are Nambu–Goldstone modes [52] associated with the spontaneous breaking of rotation symmetry of the magnetization or Néel vector. The stability of these modes implies that their damping arises only from weak anisotropic terms in the spin Hamiltonian induced by spin-orbit or dipole-dipole interaction. In contrast, long-range magnetic order is forbidden in two-dimensional Heisenberg magnets at finite temperature [53], rendering this argument inapplicable. In two dimensions, both the existence of magnetic order and the scattering of $\mathbf{k} = 0$ acoustic magnons are controlled by anisotropy, leading to magnon–magnon damping that is effectively independent of the spin–orbit coupling strength.

Interestingly, even in bulk YIG, the calculated magnon–magnon damping exceeds the magnon–phonon contribution over most of the relevant temperature range. Its absolute value at room temperature ($\sim 7 \times 10^{-5}$) is comparable to that measured experimentally in many high-quality YIG samples [13–15]. In contrast, the magnon–phonon damping is weaker ($\sim 10^{-7}$) and agrees with previous theoretical estimates [40, 41] (see SI [49] for details of the comparison). However, because the magnon–magnon damping is non-Gilbert, it cannot be used to explain FMR experiments with conventional analysis methods.

The enhanced magnon damping due to

magnon–magnon interactions may pose a critical challenge for the miniaturization of magnonic devices, particularly for applications based on monolayers of van der Waals magnetic materials. One potential strategy to mitigate this effect is the application of external magnetic fields, since the damping is non-Gilbert and α is significantly suppressed even at moderate fields. The provided *MagnoFallas* code enables the calculation of damping for any material given its spin Hamiltonian and the characteristics of the magnon–phonon interaction.

V. ACKNOWLEDGEMENTS

We thank Andrey Rybakov and Philipp Pirro for helpful discussions.

The authors acknowledge financial support from the European Union (ERC-2021-StG-101042680 2D-SMARTIES), the Spanish Government MCIU (PID2024-162182NAI00 2D- MAGIC), the María de Maeztu Centre of Excellence Program CEX2024-001467-M funded by MICIU/AEI/10.13039/501100011033, and the Generalitat Valenciana (grant CIDEXG/2023/1). A.M.R. thanks the Spanish MIU (Grant No FPU21/04195).

Appendix A: General properties of the Boltzmann formalism

The most general expression for γ_0 within the Boltzmann formalism

$$\gamma_0 = \frac{2\pi}{\hbar} \sum_{i,f} |W_{if}^2| (\mathcal{N}_> - \mathcal{N}_<) \delta(E_i - E_f) \quad (\text{A1})$$

involves a set of the initial states i and the final states f with one less $\mathbf{k} = 0$ acoustic magnon. W_{if} is the matrix element of the Hamiltonian related to the transition from i to f , $\mathcal{N}_>$ and $\mathcal{N}_<$ describe the occupation numbers of thermal phonons and magnons relevant for the direct and reversed process, respectively. Dirac delta function $\delta(E_i - E_f)$ shows that the total energy of the initial state E_i equals the energy of the final state E_f .

Because of the energy conservation law, when $\Delta \ll T$ the term $\mathcal{N}_> - \mathcal{N}_<$ can be given by the expression [49]:

$$\mathcal{N}_> - \mathcal{N}_< = \frac{\Delta}{T} \frac{\prod_A e^{\varepsilon_A/T}}{\prod_A (e^{\varepsilon_A/T} - 1) \prod_C (e^{\varepsilon_C/T} - 1)} \quad (\text{A2})$$

Here index A runs over all the quasi-particle annihilated in the process apart from the $\mathbf{k} = 0$ acoustic magnon and C denoted the quasi-particles created in the process. ε_A and ε_C are the corresponding quasi-particle energies. Eq. (A2) shows that Eq. (A1) leads to a Gilbert damping when (I) the energies of all the participating quasi-particles are large compared to Δ and are not strongly modified by the magnetic field and (II) the magnetic field dependence of W_{if} can be neglected. It happens in the

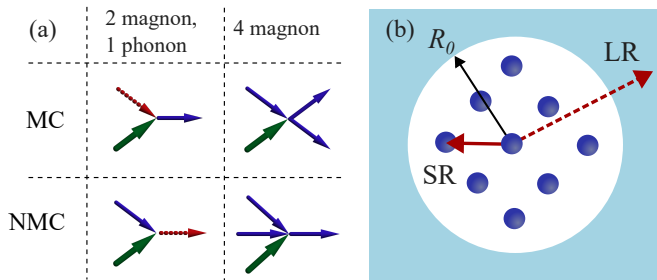


FIG. 3. (a) The processes responsible for damping. Color code: green arrow - $\mathbf{k} = 0$ acoustic magnon; blue arrows—thermal magnons; red arrows—phonons. (b) Illustration of the separation of the dipole-dipole interaction into short-range (SR) and long-range (LR) contributions.

case of magnon-phonon interaction but not of magnon-magnon interaction which is controlled by magnons with energies close to Δ .

In this work we consider four distinct processes leading to the relaxation of the $\mathbf{k} = 0$ acoustic mode: MC and MNC 2-magnon 1-phonon and 4-magnon processes shown in Fig. 3(a). All the four processes are included into the simulation of YIG and a monolayer of CrSBr, however, only MC processes are possible in the toy model. The detailed expression for W_{if} relevant for all the processes are provided in SI [49]. While 3-magnon processes are possible in the studied materials, the corresponding energy conservation laws require adsorption of high-energy magnons leading to the contribution of 3-magnon processes being negligible at relevant temperatures.

Appendix B: Details of the numerical computations

Although magnons in insulators can be viewed as collective electronic excitations [54–56], we base our modeling on spin Hamiltonians derived from *ab initio* calculations.

Ab initio simulations of YIG and monolayer CrSBr were performed using VASP [57] and SIESTA [58] codes. Tight-binding Hamiltonians were constructed with wannier90 [59], and spin Hamiltonians were derived via perturbation theory using TB2J [60] software. The resulting magnon dispersions agree well with previously reported results [51, 61]. Phonon calculations were carried out using the finite-displacement method implemented in phonopy [62]. Spin-orbit coupling was included for CrSBr, whereas YIG was treated in the non-relativistic limit. Consequently, damping in YIG arises solely from dipole-dipole interactions added at the post-processing stage.

The damping coefficient α is computed numerically using our *MagnoFallas* package, available on <https://github.com/AndreiShumilin/MagnoFallas> and described in detail in the SI [49]. Below, we summarize the key elements of its algorithms.

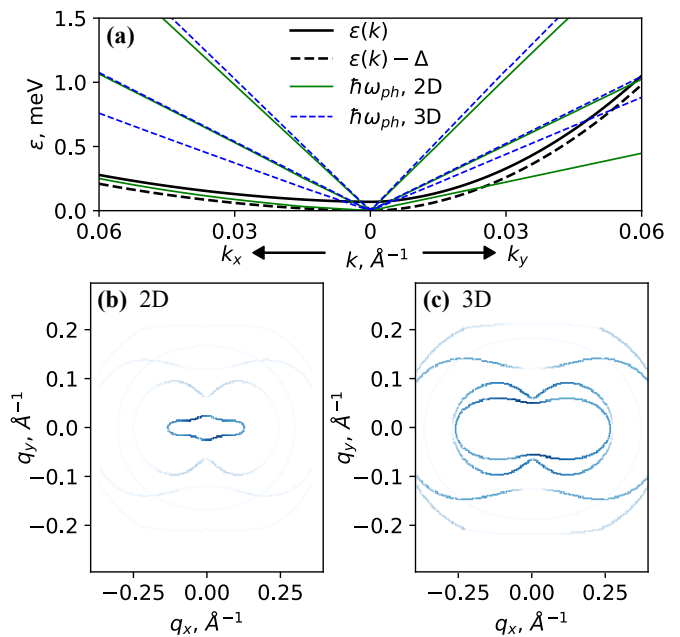


FIG. 4. (a) Low-energy magnon dispersion (black solid line) compared with the phonon dispersions obtained from *ab initio* calculations for a CrSBr monolayer (green solid line) and bulk CrSBr (blue dashed line). The black dashed line indicates the phonon energy that must be absorbed in the MC process. (b) Contributions of phonons with different wavevectors to the MC magnon-phonon damping in the case of two-dimensional phonons. (c) Corresponding contributions for three-dimensional phonons.

(I) Since W_{if} in Eq. (A2) vanishes in the non-relativistic limit when energy and momentum conservation laws are fulfilled, but remains finite for arbitrary quasiparticle wave vectors, we evaluate W_{if} only at points satisfying the conservation laws (*scattering events*). To this end, the Brillouin zone is discretized into a k -grid. For each grid cell containing valid events, we select a representative point, compute W_{if} for the corresponding wave vectors, and estimate the integral over the Dirac delta function using the marching-cubes method [63].

(II) Although dipole-dipole interactions can, in principle, be incorporated into Eq. (1) as additional terms, this approach is practical only for a limited number of neighboring spins. Nevertheless, long-range dipole-dipole interactions play an important role in magnon dynamics and must be included in the calculations. To this end, we introduce a cutoff distance R_0 that separates the dipole-dipole interaction into short- and long-range contributions according to the interspin distance r (Fig. 3(b)). Short-range interactions ($r < R_0$) are treated explicitly within the spin Hamiltonian (1). The long-range contribution is accounted for by coupling each spin to an averaged magnetization density, which allows for an analytical evaluation of its effect. Our treatment assumes spherically symmetric boundary conditions at

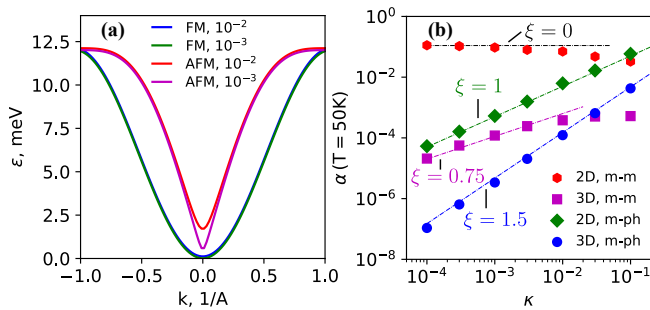


FIG. 5. (a) Comparison of the magnon dispersion of the ferromagnetic (FM) and antiferromagnetic (AFM) toy models with $\kappa = 10^{-2}$ and 10^{-3} as shown in legend. (b) Damping coefficient α at $T = 50\text{K}$ calculated for AFM toy model for different anisotropy parameters κ . The results are compared with power-law dependencies $\alpha \propto \kappa^\xi$.

large distances, corresponding to magnons near the center of a macroscopic magnetic sphere.

Appendix C: Difference between 2D and 3D phonons for the magnon-phonon damping mechanism in a monolayer of CrSBr

The pronounced difference between the damping obtained from the magnon-phonon mechanism in a CrSBr monolayer with 2D versus 3D phonons can be understood from the results shown in Fig. 4. Figure 4(a) compares

the magnon dispersion with the dispersions of 2D and 3D phonons. In the 2D case, the phonon branch corresponding to the acoustic mode with atomic displacements perpendicular to the monolayer exhibits significantly lower energies, consistent with the presence of flexural phonons [64]. As a result, crossings between the phonon and magnon spectra occur at much lower energies. Figures 4(b) and (c) show the contributions of phonons with different wavevectors to the damping for 2D and 3D phonons, respectively. In the 2D case, the damping is dominated by low-wavevector flexural phonons, which have low energies and correspondingly large occupation numbers. In contrast, for 3D phonons the damping is governed by phonons with higher energies and smaller occupation numbers, resulting in an approximately 10-fold reduction of the damping parameter α .

Appendix D: antiferromagnetic toy model

Figure 5(a) shows the magnon dispersion obtained from the toy model with antiferromagnetic exchange coupling $J = -2\text{meV}$, $\kappa = 10^{-2}$ and 10^{-3} , while all other parameters are the same as those used in Fig. 1. In contrast to the quadratic dispersion of the ferromagnetic toy model, the antiferromagnetic magnon spectrum becomes linear in k at small κ . Figure 5(b) presents the numerically calculated damping parameter α for this model at $T = 50\text{K}$ and for different values of κ . As in the ferromagnetic case, magnon-magnon scattering in the two-dimensional model remains unsuppressed at low κ , resulting in a finite damping even in this limit.

- [1] A. Barman, G. Gubbiotti, S. Ladak, A. O. Adeyeye, M. Krawczyk, J. Gräfe, C. Adelman, S. Coto-fana, A. Naeemi, V. I. Vasyuchka, B. Hillebrands, S. A. Nikitov, H. Yu, D. Grundler, A. V. Sadovnikov, A. A. Grachev, S. E. Sheshukova, J.-Y. Duquesne, M. Marangolo, G. Csaba, W. Porod, V. E. Demidov, S. Urazhdin, S. O. Demokritov, E. Albisetti, D. Petti, R. Bertacco, H. Schultheiss, V. V. Kruglyak, V. D. Poimanov, S. Sahoo, J. Sinha, H. Yang, M. Münzenberg, T. Moriyama, S. Mizukami, P. Landeros, R. A. Gallardo, G. Carlotti, J.-V. Kim, R. L. Stamps, R. E. Camley, B. Rana, Y. Otani, W. Yu, T. Yu, G. E. W. Bauer, C. Back, G. S. Uhrig, O. V. Dobrovolskiy, B. Budinska, H. Qin, S. van Dijken, A. V. Chumak, A. Khitun, D. E. Nikonov, I. A. Young, B. W. Zingsem, and M. Winklhofer, The 2021 magnonics roadmap, *Journal of Physics: Condensed Matter* **33**, 413001 (2021).
- [2] B. Flebus, D. Grundler, B. Rana, Y. Otani, I. Barsukov, A. Barman, G. Gubbiotti, P. Landeros, J. Akerman, U. Ebels, P. Pirro, V. E. Demidov, K. Schultheiss, G. Csaba, Q. Wang, F. Ciubotaru, D. E. Nikonov, P. Che, R. Hertel, T. Ono, D. Afanasiev, J. Mentink, T. Rasing, B. Hillebrands, S. V. Kusminskiy, W. Zhang, C. R. Du, A. Finco, T. van der Sar, Y. K. Luo, Y. Shiota, J. Skle-

- nar, T. Yu, and J. Rao, The 2024 magnonics roadmap, *Journal of Physics: Condensed Matter* **36**, 363501 (2024).
- [3] A. V. Chumak, P. Kabos, M. Wu, C. Abert, C. Adelman, A. O. Adeyeye, J. Åkerman, F. G. Aliev, A. Anane, A. Awad, C. H. Back, A. Barman, G. E. W. Bauer, M. Becherer, E. N. Beginin, V. A. S. V. Bittencourt, Y. M. Blanter, P. Bortolotti, I. Boventer, D. A. Bozhko, S. A. Bunyaev, J. J. Carmiggelt, R. R. Cheenikundil, F. Ciubotaru, S. Coto-fana, G. Csaba, O. V. Dobrovolskiy, C. Dubs, M. Elyasi, K. G. Fripp, H. Fulara, I. A. Golovchanskiy, C. Gonzalez-Ballester, P. Graczyk, D. Grundler, P. Gruszecki, G. Gubbiotti, K. Guslienko, A. Haldar, S. Hamdioui, R. Hertel, B. Hillebrands, T. Hioki, A. Houshang, C.-M. Hu, H. Huebl, M. Huth, E. Iacocca, M. B. Jungfleisch, G. N. Kakazei, A. Khitun, R. Khymyn, T. Kikkawa, M. Kläui, O. Klein, J. W. Klos, S. Knauer, S. Koraltan, M. Kostylev, M. Krawczyk, I. N. Krivorotov, V. V. Kruglyak, D. Lachance-Quirion, S. Ladak, R. Lebrun, Y. Li, M. Lindner, R. Macêdo, S. Mayr, G. A. Melkov, S. Mieszczak, Y. Nakamura, H. T. Nembach, A. A. Nikitin, S. A. Nikitov, V. Novosad, J. A. Otálora, Y. Otani, A. Papp, B. Pigeau, P. Pirro, W. Porod, F. Porrati, H. Qin, B. Rana, T. Reimann, F. Riente,

- O. Romero-Isart, A. Ross, A. V. Sadovnikov, A. R. Safin, E. Saitoh, G. Schmidt, H. Schultheiss, K. Schultheiss, A. A. Serga, S. Sharma, J. M. Shaw, D. Suess, O. Surzhenko, K. Szulc, T. Taniguchi, M. Urbánek, K. Usami, A. B. Ustinov, T. van der Sar, S. van Dijken, V. I. Vasyuchka, R. Verba, S. V. Kusminskiy, Q. Wang, M. Weides, M. Weiler, S. Wintz, S. P. Wolfski, and X. Zhang, *Advances in magnetism roadmap on spin-wave computing*, *IEEE Transactions on Magnetics* **58**, 1 (2022).
- [4] Á. Papp, W. Porod, and G. Csaba, *Nanoscale neural network using non-linear spin-wave interference*, *Nature Communications* **12**, 6422 (2021).
- [5] V. Vlaminck and M. Bailleul, *Current-induced spin-wave doppler shift*, *Science* **322**, 410 (2008), <https://www.science.org/doi/pdf/10.1126/science.1162843>.
- [6] B. Huang, G. Clark, E. Navarro-Moratalla, D. R. Klein, R. Cheng, K. L. Seyler, D. Zhong, E. Schmidgall, M. A. McGuire, D. H. Cobden, W. Yao, D. Xiao, P. Jarillo-Herrero, and X. Xu, *Layer-dependent ferromagnetism in a van der waals crystal down to the monolayer limit*, *Nature* **546**, 270 (2017).
- [7] T. Gilbert, *A phenomenological theory of damping in ferromagnetic materials*, *IEEE Transactions on Magnetics* **40**, 3443 (2004).
- [8] A. Aharoni, *Introduction to the Theory of Ferromagnetism* (Clarendon Press, Oxford, 1996).
- [9] T. Brächer, P. Pirro, and B. Hillebrands, *Parallel pumping for magnon spintronics: Amplification and manipulation of magnon spin currents on the micron-scale*, *Physics Reports* **699**, 1 (2017), *parallel pumping for magnon spintronics: Amplification and manipulation of magnon spin currents on the micron-scale*.
- [10] D. Breitbach, M. Schneider, B. Heinz, F. Kohl, J. Maskill, L. Scheuer, R. O. Serha, T. Brächer, B. Lägell, C. Dubs, V. S. Tiberkevich, A. N. Slavin, A. A. Serga, B. Hillebrands, A. V. Chumak, and P. Pirro, *Stimulated amplification of propagating spin waves*, *Phys. Rev. Lett.* **131**, 156701 (2023).
- [11] B. Divinskiy, V. E. Demidov, S. Urazhdin, R. Freeman, A. B. Rinkevich, and S. O. Demokritov, *Excitation and amplification of spin waves by spin-orbit torque*, *Advanced Materials* **30**, 1802837 (2018).
- [12] S. Geller and M. Gilleo, *The crystal structure and ferromagnetism of yttrium-iron garnet, $\gamma\text{-Fe}_2(\text{FeO}_4)_3$* , *Journal of Physics and Chemistry of Solids* **3**, 30 (1957).
- [13] H. Chang, P. Li, W. Zhang, T. Liu, A. Hoffmann, L. Deng, and M. Wu, *Nanometer-thick yttrium iron garnet films with extremely low damping*, *IEEE Magnetics Letters* **5**, 1 (2014).
- [14] H. Maier-Flaig, S. Klingler, C. Dubs, O. Surzhenko, R. Gross, M. Weiler, H. Huebl, and S. T. B. Goennenwein, *Temperature-dependent magnetic damping of yttrium iron garnet spheres*, *Phys. Rev. B* **95**, 214423 (2017).
- [15] G. Schmidt, C. Hauser, P. Trempler, M. Paleschke, and E. T. Papaioannou, *Ultra thin films of yttrium iron garnet with very low damping: A review*, *physica status solidi (b)* **257**, 1900644 (2020).
- [16] P. Pirro, V. I. Vasyuchka, A. A. Serga, and B. Hillebrands, *Advances in coherent magnonics*, *Nature Reviews Materials* **6**, 1114 (2021).
- [17] M. E. Ziebel, M. L. Feuer, J. Cox, X. Zhu, C. R. Dean, and X. Roy, *Crsbr: An air-stable, two-dimensional magnetic semiconductor*, *Nano Letters* **24**, 4319 (2024).
- [18] D. K. de Wal, A. Iwens, T. Liu, P. Tang, G. E. W. Bauer, and B. J. van Wees, *Long-distance magnon transport in the van der waals antiferromagnet crps_4* , *Phys. Rev. B* **107**, L180403 (2023).
- [19] V. Kamberský, *Spin-orbital gilbert damping in common magnetic metals*, *Phys. Rev. B* **76**, 134416 (2007).
- [20] M. C. Hickey and J. S. Moodera, *Origin of intrinsic gilbert damping*, *Phys. Rev. Lett.* **102**, 137601 (2009).
- [21] A. A. Pervishko, M. I. Baglai, O. Eriksson, and D. Yudin, *Another view on gilbert damping in two-dimensional ferromagnets*, *Scientific Reports* **8**, 17148 (2018).
- [22] A. G. Gurevich and G. A. Melkov, *Magnetization Oscillations and Waves*, 1st ed. (CRC Press, Boca Raton, FL, 2020).
- [23] X. Xu, L. Zheng, L. Jin, T. Wen, Y. Liao, X. Tang, H. Zhang, and Z. Zhong, *Tunable non-gilbert-type damping in $\text{ni}_{80}\text{fe}_{20}$ films sputtered on the rippled al_2o_3 substrates*, *Journal of Alloys and Compounds* **893**, 162319 (2022).
- [24] S. Emori, U. S. Alaán, M. T. Gray, V. Sluka, Y. Chen, A. D. Kent, and Y. Suzuki, *Spin transport and dynamics in all-oxide perovskite $\text{la}_{2/3}\text{sr}_{1/3}\text{mno}_3/\text{srruo}_3$ bilayers probed by ferromagnetic resonance*, *Phys. Rev. B* **94**, 224423 (2016).
- [25] H. K. Lee, I. Barsukov, A. G. Swartz, B. Kim, L. Yang, H. Y. Hwang, and I. N. Krivorotov, *Magnetic anisotropy, damping, and interfacial spin transport in pt/lsmo bilayers*, *AIP Advances* **6**, 055212 (2016).
- [26] J. Lindner, K. Lenz, E. Kosubek, K. Baberschke, D. Spoddig, R. Meckenstock, J. Pelzl, Z. Frait, and D. L. Mills, *Non-gilbert-type damping of the magnetic relaxation in ultrathin ferromagnets: Importance of magnon-magnon scattering*, *Phys. Rev. B* **68**, 060102 (2003).
- [27] G. Woltersdorf and B. Heinrich, *Two-magnon scattering in a self-assembled nanoscale network of misfit dislocations*, *Phys. Rev. B* **69**, 184417 (2004).
- [28] K. Lenz, H. Wende, W. Kuch, K. Baberschke, K. Nagy, and A. Jánossy, *Two-magnon scattering and viscous gilbert damping in ultrathin ferromagnets*, *Phys. Rev. B* **73**, 144424 (2006).
- [29] S. Iihama, A. Sakuma, H. Naganuma, M. Oogane, S. Mizukami, and Y. Ando, *Influence of l_{10} order parameter on gilbert damping constants for fepd thin films investigated by means of time-resolved magneto-optical kerr effect*, *Phys. Rev. B* **94**, 174425 (2016).
- [30] R. Salikhov, A. Alekhin, T. Parpiiev, T. Pezeril, D. Makarov, R. Abrudan, R. Meckenstock, F. Radu, M. Farle, H. Zabel, and V. V. Temnov, *Gilbert damping in nifegd compounds: Ferromagnetic resonance versus time-resolved spectroscopy*, *Phys. Rev. B* **99**, 104412 (2019).
- [31] H. Gao, J. Lu, J. Zhao, and X. Zhang, *Magnetization dynamics and gilbert damping in a hybrid fe/gaas heterostructure*, *Solid State Communications* **192**, 31 (2014).
- [32] G. Woltersdorf, M. Kiessling, G. Meyer, J.-U. Thiele, and C. H. Back, *Damping by slow relaxing rare earth impurities in $\text{ni}_{80}\text{fe}_{20}$* , *Phys. Rev. Lett.* **102**, 257602 (2009).
- [33] C. L. Jermain, S. V. Aradhya, N. D. Reynolds, R. A. Buhrman, J. T. Brangham, M. R. Page, P. C. Hammel, F. Y. Yang, and D. C. Ralph, *Increased low-temperature*

- damping in yttrium iron garnet thin films, *Phys. Rev. B* **95**, 174411 (2017).
- [34] H. Ebert, S. Mankovsky, D. Ködderitzsch, and P. J. Kelly, Ab initio calculation of the gilbert damping parameter via the linear response formalism, *Phys. Rev. Lett.* **107**, 066603 (2011).
- [35] E. Barati, M. Cinal, D. M. Edwards, and A. Umerski, Gilbert damping in magnetic layered systems, *Phys. Rev. B* **90**, 014420 (2014).
- [36] J. Wang, S.-B. Zhao, J.-w. Li, L. Zhuang, and Y. Hou, Highly tunable gilbert damping in the two-dimensional van der waals ferromagnet Fe_3GaTe_2 : From bilayer to twisted bilayer, *Phys. Rev. B* **112**, 094448 (2025).
- [37] L. Hong, C. Xu, and H. Xiang, Evaluating gilbert damping in magnetic insulators from first-principles, *Phys. Rev. B* **109**, 094429 (2024).
- [38] A. Cong, J. Liu, W. Xue, H. Liu, Y. Liu, and K. Shen, Exchange-mediated magnon-phonon scattering in monolayer CrI_3 , *Phys. Rev. B* **106**, 214424 (2022).
- [39] V. A. Shklovskiy, V. V. Mezinova, and O. V. Dobrovolskiy, Nonlinear relaxation between magnons and phonons in insulating ferromagnets, *Phys. Rev. B* **98**, 104405 (2018).
- [40] S. Streib, N. Vidal-Silva, K. Shen, and G. E. W. Bauer, Magnon-phonon interactions in magnetic insulators, *Phys. Rev. B* **99**, 184442 (2019).
- [41] A. Rückriegel, P. Kopietz, D. A. Bozhko, A. A. Serga, and B. Hillebrands, Magnetoelastic modes and lifetime of magnons in thin yttrium iron garnet films, *Phys. Rev. B* **89**, 184413 (2014).
- [42] K. Wang, X. Xu, Y. Cheng, M. Zhang, J.-S. Wang, H. Wang, and G. Zhang, Magnon-magnon interaction and magnon relaxation time in a ferromagnetic $\text{Cr}_2\text{Ge}_2\text{Te}_6$ monolayer, *Phys. Rev. B* **102**, 235434 (2020).
- [43] D. Luo, A. Cong, S. Wen, Z. Yuan, K. Shen, and Y. Liu, Magnon-magnon scattering in monolayer CrI_3 , *Phys. Rev. B* **111**, 094430 (2025).
- [44] S. M. Rezende and R. M. White, Multimagnon theory of antiferromagnetic resonance relaxation, *Phys. Rev. B* **14**, 2939 (1976).
- [45] S. P. Bayraktci, D. A. Tennant, P. Leininger, T. Keller, M. C. R. Gibson, S. D. Wilson, R. J. Birgeneau, and B. Keimer, Lifetimes of antiferromagnetic magnons in two and three dimensions: Experiment, theory, and numerics, *Phys. Rev. Lett.* **111**, 017204 (2013).
- [46] L. D. Landau, E. M. Lifshitz, and L. P. Pitaevskii, *Physical Kinetics*, Course of Theoretical Physics, Vol. 10 (Butterworth-Heinemann, Oxford, 1981) translated from the Russian by J. B. Sykes and R. N. Franklin.
- [47] S. Toth and B. Lake, Linear spin wave theory for single-q incommensurate magnetic structures, *Journal of Physics: Condensed Matter* **27**, 166002 (2015).
- [48] T. Holstein and H. Primakoff, Field dependence of the intrinsic domain magnetization of a ferromagnet, *Phys. Rev.* **58**, 1098 (1940).
- [49] The Supporting Information includes the derivation of the analytical results presented in the article, a detailed description of the numerical algorithms, and additional details on the simulation of damping in YIG and in a monolayer of CrSBr.
- [50] A. Scheie, M. Ziebel, D. G. Chica, Y. J. Bae, X. Wang, A. I. Kolesnikov, X. Zhu, and X. Roy, Spin waves and magnetic exchange hamiltonian in crsbr, *Advanced Science* **9**, 2202467 (2022).
- [51] D. L. Esteras, A. Rybakov, A. M. Ruiz, and J. J. Baldoví, Magnon straintronics in the 2d van der waals ferromagnet crsbr from first-principles, *Nano Letters* **22**, 8771 (2022).
- [52] H. Watanabe, Counting rules of nambu-goldstone modes, *Annual Review of Condensed Matter Physics* **11**, 169 (2020).
- [53] N. D. Mermin and H. Wagner, Absence of ferromagnetism or antiferromagnetism in one- or two-dimensional isotropic heisenberg models, *Phys. Rev. Lett.* **17**, 1133 (1966).
- [54] F. Aryasetiawan and K. Karlsson, Green's function formalism for calculating spin-wave spectra, *Phys. Rev. B* **60**, 7419 (1999).
- [55] K. B. Le, A. Esquembre-Kučukalić, H.-Y. Chen, I. Maliyov, Y. Luo, J.-J. Zhou, D. Sangalli, A. Molina-Sánchez, and M. Bernardi, Magnon-phonon interactions from first principles, *Phys. Rev. B* **112**, L180403 (2025).
- [56] A. Esquembre-Kučukalić, K. B. Le, A. García-Cristóbal, M. Bernardi, D. Sangalli, and A. Molina-Sánchez, Magnons in chromium trihalides calculated with the ab initio bethe-salpeter equation, *Phys. Rev. B* **112**, 184412 (2025).
- [57] G. Kresse and J. Furthmüller, Efficient iterative schemes for ab initio total-energy calculations using a plane-wave basis set, *Phys. Rev. B* **54**, 11169 (1996).
- [58] J. M. Soler, E. Artacho, J. D. Gale, A. García, J. Junquera, P. Ordejón, and D. Sánchez-Portal, The siesta method for ab initio order-n materials simulation, *Journal of Physics: Condensed Matter* **14**, 2745 (2002).
- [59] G. Pizzi, V. Vitale, R. Arita, S. Blügel, F. Freimuth, G. Géranton, M. Gibertini, D. Gresch, C. Johnson, T. Koretsune, J. Ibañez-Azpiroz, H. Lee, J.-M. Lihm, D. Marchand, A. Marrazzo, Y. Mokrousov, J. I. Mustafa, Y. Nohara, Y. Nomura, L. Paulatto, S. Poncé, T. Ponweiser, J. Qiao, F. Thöle, S. S. Tsirkin, M. Wierzbowska, N. Marzari, D. Vanderbilt, I. Souza, A. A. Mostofi, and J. R. Yates, Wannier90 as a community code: new features and applications, *Journal of Physics: Condensed Matter* **32**, 165902 (2020).
- [60] X. He, N. Helbig, M. J. Verstraete, and E. Bousquet, Tb2j: A python package for computing magnetic interaction parameters, *Computer Physics Communications* **264**, 107938 (2021).
- [61] O. I. Gorbatov, G. Johansson, A. Jakobsson, S. Mankovsky, H. Ebert, I. Di Marco, J. Minár, and C. Etz, Magnetic exchange interactions in yttrium iron garnet: A fully relativistic first-principles investigation, *Phys. Rev. B* **104**, 174401 (2021).
- [62] A. Togo and I. Tanaka, First principles phonon calculations in materials science, *Scripta Materialia* **108**, 1 (2015).
- [63] W. E. Lorensen and H. E. Cline, Marching cubes: a high resolution 3d surface construction algorithm, in *Seminal Graphics: Pioneering Efforts That Shaped the Field, Volume 1* (Association for Computing Machinery, New York, NY, USA, 1998) p. 347-353.
- [64] L. D. Landau, L. P. Pitaevskii, A. M. Kosevich, and E. M. Lifshitz, *Theory of Elasticity: Volume 7 (Course of Theoretical Physics)*, 3rd ed., Course of Theoretical Physics (Elsevier Butterworth Heinemann, Oxford; New York, 1986).